Nano Research 2017, 10(1): 49–63
DOI 10.1007/s12274-016-1265-9
Research Article

ISSN 1998-0124
CN 11-5974/O4

Optimizing surface-engineered ultra-small gold nanoparticles for highly efficient miRNA delivery to enhance osteogenic differentiation of bone mesenchymal stromal cells

Meng Yu[1,§], Bo Lei[1,2,3,§] (✉), Chuanbo Gao[1], Jin Yan[1], and Peter X. Ma[4,5,6] (✉)

[1] *Frontier Institute of Science and Technology, Xi'an Jiaotong University, Xi'an 710054, China*
[2] *State Key Laboratory for Manufacturing Systems Engineering, Xi'an Jiaotong University, Xi'an 710054, China*
[3] *State Key Laboratory for Mechanical Behavior of Materials, Xi'an Jiaotong University, Xi'an 710054, China*
[4] *Department of Biomedical Engineering, University of Michigan, Ann Arbor, MI 48109-2009, USA*
[5] *Macromolecular Science and Engineering Center, University of Michigan, Ann Arbor, MI 48109-1055, USA*
[6] *Department of Materials Science and Engineering, University of Michigan, Ann Arbor, MI 48109-1078, USA*
[§] *These authors contributed equally to this work.*

Received: 27 June 2016
Revised: 16 August 2016
Accepted: 26 August 2016

KEYWORDS
ultra-small gold nanoparticles,
surface engineering,
microRNA (miRNA) delivery,
bone mesenchymal stromal cells,
osteogenic differentiation

ABSTRACT

Regulation of osteogenic differentiation of bone mesenchymal stromal cells (BMSCs) plays a critical role in bone regeneration. As small non-coding RNAs, microRNAs (miRNAs) play an important role in stem cell differentiation through regulating target-mRNA expression. Unfortunately, highly efficient and safe delivery of miRNAs to BMSCs to regulate their osteogenic differentiation remains challenging. Conventional inorganic nanocrystals have shown increased toxicity owing to their larger size precluding renal clearance. Here, we developed novel, surface-engineered, ultra-small gold nanoparticles (USAuNPs, <10 nm) for use as highly efficient miR-5106-delivery systems to enable regulation of BMSC differentiation. We exploited the effects of AuNPs coated layer-by-layer with polyethylenimine (PEI) and liposomes (Lipo) to enhance miR-5106-delivery activity and subsequent BMSC differentiation capacity. The PEI- and Lipo-coated AuNPs (Au@PEI@Lipo) showed negligible cytotoxicity, good miRNA-5106-binding affinity, highly efficient delivery of miRNAs to BMSCs, and long-term miRNA expression (21 days). Additionally, compared with commercial Lipofectamine 3000 and 25 kD PEI, the optimized Au@PEI@Lipo-miR-5106 nanocomplexes significantly enhanced BMSC differentiation into osteoblast-like cells through activation of the *Sox*9 transcription factor. Our findings reveal a promising strategy for the rational design of ultra-small inorganic nanoparticles as highly efficient miRNA-delivery platforms for tissue regeneration and disease therapy.

Address correspondence to Bo Lei, rayboo@xjtu.edu.cn, leiboaray@foxmail.com; Peter X. Ma, mapx@umich.edu

1 Introduction

As progenitor cells, bone mesenchymal stromal cells (BMSCs) can differentiate into various tissue cells under suitable microenvironments and exhibit promising applications in tissue regeneration and disease therapy [1]. Directing BMSC-differentiation fate is important for successful tissue engineering [2]. MicroRNAs (miRNA) are a class of single-stranded RNAs consisting of 18 to 22 nucleotide base pairs, and play important roles in regulating biological processes, including controlling gene transcription through the activation or degradation of target mRNA [3]. Therefore, as functional biomolecules, various miRNAs have been employed to regenerate bone tissue and treat diseases [4–6]. Subsequently, many positive results have been reported through delivery of miRNAs into tissue-regeneration sites and targeted cells.

However, cell uptake of naked miRNAs through the cell membrane is difficult owing to their similar charge (negatively charged). Additionally, naked miRNAs are also rapidly degraded *in vivo* [7]. Therefore, highly efficient and minimally toxic vehicles are necessary to protect and deliver miRNA into target cells. Viruses and liposomes have been widely studied as gene vectors; however, they continue to show disadvantages such as instability in the blood and the ability to trigger immune responses [8, 9]. Artificial cationic polyethylenimine (PEI) has been used as a non-viral vector to deliver miRNA both *in vitro* and *in vivo* [10, 11]. Unfortunately, despite its good transfection efficiency, high-molecular-weight (25 kD) PEI exhibits high levels of cytotoxicity, whereas low-molecular-weight PEI (<2 kD) exhibits negligible cytotoxicity, but low transfection efficiency [12, 13]. Although developing novel miRNA-delivery systems with highly efficient transfection ability and minimal cytotoxicity has attracted much attention in the fields of tissue regeneration and cancer therapy [14–16], few low-cost, facile polymer miRNA vectors exhibiting higher transfection efficiencies than those associated with 25 kD PEI have been developed [17].

Gold nanoparticles (AuNPs) are considered promising non-viral gene-delivery vectors owing to their facile synthesis, controlled size distribution, good biocompatibility, and easy surface functionalization [18–20]. Biofunctionalized AuNPs were employed to successfully protect and deliver genes, as well as DNA, small interfering RNA (siRNA), and miRNA [21–23]. However, conventional AuNPs used for gene delivery usually possess a large size distribution (>10 nm) and may accumulate in different tissues owing to difficulty in renal clearance, which has increased concerns regarding the long-term toxicity of AuNPs [24–26]. By contrast, compared with conventional nanoparticles, ultra-small AuNPs (USAuNPs, <10 nm) can carry drugs or genes into target cells and reach cell nuclei easily [27]. Furthermore, recent studies showed that USAuNPs can be excreted through the kidney [28]. Therefore, use of USAuNPs as miRNA vectors for regulating BMSC growth and differentiation is a reasonable and promising strategy.

As compared with the chemical-grafting method for affixing miRNA, layer-by-layer assembly demonstrates advantages such as being a facile process and resulting in high flexibility [29, 30]. In this study, to increase the stability of Lipofectamine 3000 (Lipo), decrease PEI toxicity, and utilize the advantages of USAuNPs, we optimized the surface function of USAuNPs for miRNA delivery through layer-by-layer assembly of PEI and Lipo. Our results indicate that the optimized Au@PEI@Lipo nanoplatforms has high cellular biocompatibility (relative to that of PEI), improved miR-5106-delivery efficiency (relative to that observed from Lipo), and significantly enhanced BMSC osteogenic differentiation. We also investigated the mechanisms associated with miR-5106-delivered enhancement of BMSC osteogenic differentiation.

2 Experimental

2.1 Materials

Branched PEI (25 kD), hydrogen tetrachloroaurate (III) trihydrate ($HAuCl_4 \cdot 3H_2O$), trisodium citrate dihydrate, 16-mercaptohexadecanoic acid (MHA), ascorbic acid, α-glycerophosphate, paraformaldehyde, Triton X-100, dexamethasone, and sodium borohydride ($NaBH_4$, 99%) were purchased from Sigma-Aldrich (St. Louis, MO, USA). Lipo was purchased from Thermo Fisher Scientific (Waltham, MA, USA). All chemicals were used as received without further purification. Other

biological chemicals were obtained from Thermo Fisher Scientific if not specified. 5,6-Carboxyfluorescein (FAM)-labeled miR-5106 was purchased from GenePharma (Shanghai, China).

2.2 USAuNP synthesis

The USAuNPs were synthesized according to a previous report [31]. Briefly, 1 mL $HAuCl_4$ (Au salt, 5 mM) and 1 mL trisodium citrate dehydrate (capping agent, 5 mM) were mixed with 18 mL H_2O in a flask. Under vigorous stirring, 0.6 mL $NaBH_4$ solution (0.1 M) was quickly injected into the solution. The gold-colloidal solution was stirred for an additional 8 h, and the AuNPs were collected by centrifugation and re-dispersed in water. To obtain a negatively charged surface, the trisodium citrate-capped AuNPs were dispersed in 1 M NaOH (pH 11), followed by addition of MHA. The MHA-stabilized AuNPs were purified by centrifugation and washing and resuspended in phosphate-buffered saline (PBS).

2.3 Fabrication of Au@PEI@Lipo nanoparticles

Au@PEI@Lipo nanoparticles were fabricated by layer-by-layer self-assembly technology. Briefly, carboxyl-capped AuNPs were added into the PEI (1 mg/mL) and Lipo (1 mg/mL) solutions for coating and self-assembling, respectively (Au@PEI and Au@Lipo). Each coating step for PEI and Lipo was performed for 30 min. The Au@PEI@Lipo system was obtained by adding AuNPs into the PEI and Lipo mixture solutions (at the same volumes) and incubating for 30 min. After adsorption, the AuNPs were washed with deionized water three times, and the coated Au@PEI, Au@Lipo, and Au@PEI@Lipo nanoparticles were stored until further use.

2.4 Preparation and structure evaluation of Au@PEI@Lipo-miRNA nanocomplexes

The AuNP-miRNA nanocomplex was prepared at 37 °C in an Opti-MEM (reduced serum medium; Thermo Fisher Scientific) environment. Specifically, miRNA nanocomplexes involving Au@PEI, Au@Lipo, Au@PEI@Lipo were prepared by adding nanoparticles into the miRNA solution (0.26 mg/mL) and incubating for 30 min. The miRNA nanocomplexes were purified by centrifugation at 12,000 rpm for 20 min and resuspended in fresh Opti-MEM. The morphology of AuNPs, Au@PEI~miR-5106, Au@Lipo~miR-5106, and Au@PEI@Lipo~miR-5106 nanocomplexes was observed by transmission electron microscopy (TEM; F20; FEI, Hillsboro, OR, USA), and particle sizes were estimated from the measurement of 50 particles according to TEM results. The zeta potentials of various miR-5106 nanocomplexes were measured by dynamic light scattering (DLS; ZS90; Malvern Instruments, Malvern, UK). The UV–vis spectra of miRNA nanocomplexes dissolved in amino acid 4-(2-hydroxyethyl)-1-piperazineëthanesulfonic acid (HEPES) buffer solution (pH 6.6) were recorded from 1,100 to 200 nm, using a spectrophotometer (Lambda 35; PerkinElmer, Waltham, MA, USA).

2.5 Loading and stability analysis of Au@PEI@Lipo-miRNA nanocomplexes

The loading of and interaction between nanoparticles and miRNAs were evaluated by gel-retardation assay (Gel DOC XR+; Bio-rad, Hercules, CA, USA). Briefly, the prepared miRNA complex was dispersed in HEPES buffer solution and incubated for 30 min at 37 °C. The nanocomplex solutions were then stirred for 10 s, loaded onto a 2% agarose gel with nucleic acid gel stain (GreenviewTM; Genecopoeia, Rockville, MD, USA), and electrophoresed at 115 V. The results were visualized using a gel-imaging system (DOC XR+; Bio-Rad). The serum stability of the miRNA nanocomplexes was determined by incubation with 25% fetal bovine serum (FBS) at 37 °C for different time periods (0, 0.25, 0.5, 1, 3, 6, 12, and 24 h). The final concentration of miRNA was 2 nM. At every time point, samples were collected and analyzed by gel retardation in Tris/boric acid/EDTA electrophoretic buffer (4% agarose gel electrophoresed at 110 V for 20 min). The miRNA bands were visualized using the gel-imaging system (Gel DOC XR+, Bio-Rad), and naked miRNA was used as a control.

2.6 Cellular-biocompatibility assessment

Rat BMSCs (MT-BIO, Shanghai, China) were seeded into a 24-well plate at 1×10^4 cells/well and incubated at 37 °C in complete modified Eagle medium alpha (α-MEM; Sigma-Aldrich) containing 20% FBS under

5% CO_2 humidified atmosphere. After culture for 24 h, miRNA complexes (100 μg·mL^{-1}) were added into the wells and incubated for different time periods. Commercial PEI (25 kD) and Lipo with miRNA were used as controls. At the predetermined time points, 100 μL alamar blue reagent (Thermo Fisher Scientific) was added to each well, and the plate was incubated for 4 h. The optical density (OD) was measured at 530 nm excitation and 600 nm emission on a microreader (Spectramax; Molecular Devices, Sunnyvale, CA, USA). Untreated cells were used as controls, and cell viability was expressed as the relative cell proliferation rate $OD_{sample}/OD_{control}$.

Cell attachment and morphology were determined using a live/dead stain assay kit (Thermo Fisher Scientific). Briefly, after culture for 24 h, cells were washed with PBS, incubated in 400 μL of live/dead solution (calcein-AM and ethidium homodimer) for 45 min, and then washed three times with PBS. The fluorescent images of stained live and dead cells were obtained under a fluorescence microscope (IX53; Olympus, Tokyo, Japan).

2.7 Transfection efficiency and cell-uptake evaluation of miRNA-loaded nanoparticles

BMSCs were transfected with Au@PEI-miR-5106, Au@Lipo-miR-5106, or Au@PEI@Lipo-miR-5106 in Opti-MEM medium, with PEI-miR-5106 and Lipo-miR-5106 used as controls. Transfection efficiency was determined by fluorescence confocal microscopy (FV1200; Olympus) and quantitative real-time polymerase chain reaction (qRT-PCR; Bio-rad). Primers used for qRT-PCR are listed in Table S1 (in the Electronic Supplementary Material (ESM)). Total RNA from BMCSs was extracted with Tripure (Roche, Basel Switzerland). Single-stranded cDNAs were prepared from 0.1 μg miRNA, using a RevertAid first-strand synthesis kit (Roche). The cycle parameters were: 65 ℃ for 10 min, 25 ℃ for 25 min, 55 ℃ for 30 min, and 85 ℃ for 10 min. qRT-PCR for miRNA detection was performed in a 15-μL mixture containing 7.5 μL iTaq Universal SYBR Green supermix (Bio-rad), 6.4 μL distillation–distillation H_2O (ddH_2O), 0.5 μL template, 0.3 μL forward primer, and 0.3 μL reverse primer. The parameters were: 94 ℃ for 5 min, followed by 94 ℃ for 10 s, 58 ℃ for 30 s, and 70 ℃ for 10 s (7500 fast; Bio-rad). Flow cytometry was employed to monitor the quantitative cellular uptake of nanoparticles in BMSCs (CytoFLEX; Beckman Coulter, Brea, CA, USA). Briefly, BMSCs transfected with FAM-labeled miRNA nanoparticles for 24 h were washed with PBS three times, trypsinized, centrifuged, re-suspended in 200 μL PBS containing 2% FBS, supplemented with 200 μL 4% paraformaldehyde, and incubated at 4 ℃ for 2 h. The fluorescence-intensity distribution for samples was analyzed for 10,000 cells, using CytExpert software (Beckman Coulter).

2.8 Osteogenic differentiation and mechanism analysis

2.8.1 Alkaline phosphatase (Alp) activity

Alp activity, an early marker of osteogenic differentiation, was assessed on days 7, 14, and 21. Briefly, cells with a density of 2×10^4 cells/well were seeded into 24-well plates and transfected with various miR-5106 nanocomplexes. After incubation for 24 h at 37 ℃ and 5% CO_2, the medium was changed to differentiation medium containing 50 mg/mL ascorbic acid, 10 mM α-glycerophosphate, and 10 nM dexamethasone. At various time points, cell lysates were analyzed for Alp activity using a SensoLyte pNPP Alp assay kit (AnaSpec, Fremont, CA, USA), and Alp activity was normalized to the total protein content measured using the Pierce BCA protein assay kit (Thermo Fisher Scientific) according to manufacturer instructions. The levels of Alp activity were determined from absorbance at 405 nm using a microreader. At least four species per sample were evaluated.

2.8.2 Calcium deposition and extracellular-matrix mineralization

After osteogenic induction for 14 and 21 days following miR-5106 delivery, the calcium deposition and extracellular-matrix mineralization of cells were tested using an alizarin red stain kit (Genmed, Quebec, Canada) according to manufacturer instructions. Briefly, at the predetermined time, cells were fixed with reagent A for 20 min at room temperature, washed with PBS, and stained with reagent B for 2 h. The stained cells were detected with a fluorescence microscope (IX53; Olympus), and the calcium content of the differentiated BMSCs induced by various miRNA nanocomplexes

was estimated using an end-point colorimetry method. Briefly, BMSCs with samples were cultured in 24-well plates at a density of 2 × 10^4 cells/mL and harvested at the determined time points (day 14 and day 21). After homogenization with ddH_2O, 10 μL supernatant containing cells was added into a 96-well plate, followed by the addition of 250 μL chromogenic reagent II (Nanjing Jiancheng Bioengineering Institute, Nanjing, China). After further incubation for 5 min, the OD was measured at 610 nm by a Spectramax paradigm (Molecular Devices). The calcium content in cells was calculated according to the standard curve of calcium. At least four species per sample were tested.

2.8.3 *Immunofluorescence staining*

Cells were seeded into a 48-well plate at 5 × 10^3 cells/well and incubated in complete α-MEM containing 20% FBS under 5% CO_2 humidified atmosphere at 37 ℃. After culture for 24 h, miRNA nanocomplexes (100 μg/mL; Au@PEI-miR-5106, Au@Lipo-miR-5106, and Au@PEI@Lipo-miR-5106) were added into the media containing BMSCs and incubated for different time periods. Commercial PEI (25 kD) and Lipo were used as controls. On day 21, cells were fixed in 4% paraformaldehyde for 20 min and treated with 0.1% Triton X-100 for 15 min at room temperature. After blocking with 1% bovine serum albumin for 30 min, cells were incubated with primary antibodies against *Runx*2 (1:1,000; Abcam, Cambridge, UK) or *Ocn* (1:200; Abcam) overnight at 4 ℃. After washing three times with PBS, the appropriate secondary antibodies (Alexa 594; Thermo Fisher Scientific) were added and incubated for 1 h at 37 ℃ in the dark. Images were captured using a fluorescence microscope (IX53; Olympus).

2.8.4 *qRT-PCR*

We performed qRT-PCR analysis to validate the expression patterns of miR-5106, *Alp*, *Runx*2, *Ocn*, and *Opn*. Total RNA was extracted from BMSCs, using Tripure (Roche), and single-stranded cDNAs were prepared from 0.5 μg RNA, using a RevertAid first-strand cDNA synthesis kit (Roche). The cycle parameters were: 65 ℃ for 10 min, 25 ℃ for 25 min, 55 ℃ for 30 min, and 85 ℃ for 10 min. qRT-PCR was performed in a 15-μL mixture containing 7.5 μL iTaq universal SYBR Green supermix (Applied Biosystems 7500; Bio-rad), 6.4 μL ddH_2O, 0.5 μL cDNA template, 0.3 μL forward primer, and 0.3 μL reverse primer. The parameters were: 94 ℃ for 5 min, followed by 94 ℃ for 10 s, 58 ℃ for 30 s, and 70 ℃ for 10 s. The primers for qRT-PCR are shown in Table S1 (in the ESM).

2.8.5 *Dual-luciferase-reporter gene evaluation*

To determine the target site of miR-5106 in BMSCs, two copies of the target sequences for the *Sox*9 mRNA 3′ untranslated region (UTR) were cloned into the *Xho*I/*Not*I site of the psiCHECKTM-2 dual-luciferase vector (Ribobio, Guangzhou, China). The primers for the *Sox*9 3′UTR are listed in Table S2 (in the ESM). For luciferase-activity analysis, BMSCs were co-transfected with 100 ng of dual-luciferase reporter and 10 pmol miRNAs, with 1 μL/well Lipo added according to manufacturer instructions. After transfection for 48 h, the cells were lysed for measurement using a dual-luciferase assay system (Promega, Durham, NC, USA). Luminescence measurements were performed on a Spectramax paradigm (Molecular Devices). At least three independent experiments were performed in triplicate.

2.9 Statistical analysis

Data were presented as mean ± standard deviation. Statistical differences between two groups were determined by Student's *t*-test. A $p < 0.05$ was considered statistically significant.

3 Results and discussion

3.1 Synthesis and characterization of USAu-miRNA-based nanocomplexes

Au@PEI@Lipo nanovectors used for miR-5106 delivery were fabricated by layer-by-layer self-assembly technology (Fig. 1). As shown in Fig. 1(a), positively charged PEI (25 kD) was first coated onto the surface of carboxyl-capped USAuNPs, followed by the self-assembly of negatively charged Lipo. After loading miR-5106, the miRNA nanocomplexes were taken up by cells via PEI or Lipo (Fig. 1(b)). After release from the endosome, miR-5106 was able to attach to its target site, induce osteogenic gene expression, and enhance BMSC osteoblastic differentiation.

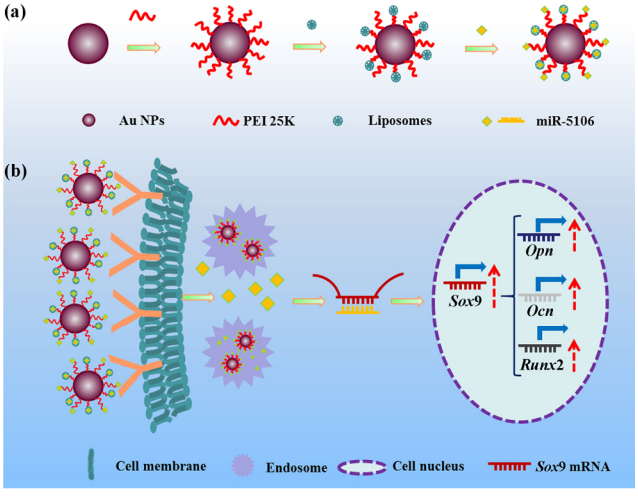

Figure 1 Illustration describing the optimization of surface-engineered USAuNPs for inducing BMSC osteogenic differentiation following miR-5106 delivery. (a) Surface engineering of USAuNPs. (b) Enhancing BMSC osteogenic differentiation by delivering miR-5106.

Characterization of the physicochemical structures of USAu-miRNA-based nanocomplexes are shown in Fig. 2. The spherical USAuNPs exhibited a mean diameter of 6.5 nm (Fig. 2(a)); however, after coating and miRNA loading, the mean diameters of Au@PEI-miR-5106, Au@Lipo-miR-5106, and Au@PEI@Lipo-miR-5106 increased to 7.8, 7.5, and 7.0 nm, respectively (Fig. 2(b)). Pure Au and PEI possessed UV–vis-absorption peaks at ~530 nm and ~285 nm, respectively (Fig. 2(c)). Au@PEI- miR-5106, Au@Lipo-miR-5106, and Au@PEI@Lipo-miR-5106 displayed similar representative absorption peaks as those of PEI and Au, demonstrating the successful coating of PEI onto the Au surface. No obvious adsorption peak representing pure Lipo and miRNA was observed. Notably, the peak Au positions showed significant red shifts after coating. Pure polymers, such as PEI, usually have poor absorbance at high wavelengths (>500 nm); however, AuNP surface plasmon resonance peaks usually show red shifts along with increases in size [32–34]. Therefore, the red shift observed at the Au-peak position should be attributed to the increase in AuNP size after coating (Fig. 2(b)). The AuNP layer-by-layer self-assembly process was also evident following zeta potential analysis (Fig. 2(d)). The zeta potentials of AuNPs, PEI, and Lipo were 2, 5, and 6 mV, respectively (Fig. 2(d)). After layer-by-layer coating, the zeta potential of Au@PEI and Au@PEI@Lipo increased to 32 and 37.5 mV, respectively. The increased positive potential for the Au complexes may constitute an additional benefit for miRNA loading and delivery. Gel-retardation assays confirmed that miR-5106 was successfully loaded onto and immobilized by Au@PEI, Au@Lipo, and Au@PEI@Lipo nanoparticles (Fig. 2(e)). The high serum stability of various miRNA-nanoparticle complexes was also indicated (Fig. 2(f)), and there were no significant differences observed between USAu-miRNA groups. These results demonstrated that nanoparticles consisting of Au, PEI, and Lipo were successfully assembled by layer-by-layer coating, and that miRNAs were successfully loaded onto and stabilized by the various nanoparticles.

3.2 Transfection and delivery of miRNAs by surface-engineered USAuNPs

The transfection and delivery of miR-5106 via USAu-based nanocomplexes were observed by laser confocal microscopy and detected by qRT-PCR, as shown in Fig. 3. After a 24-h incubation with BMSCs with FAM-labeled miRNA nanocomplexes, the strong green fluorescence associated with miR-5106 incorporation into the cells was observed, indicating that transfection was successful (Fig. 3(a)). The fluorescence intensities of Lipo-miR-5106, Au@Lipo-miR-5106, and Au@PEI@Lipo-miR-5106 were significantly stronger than those observed from other groups. The highly efficient transfection and sustained expression of miR-5106 in BMSCs were also confirmed by qRT-PCR analysis (Fig. 3(b)). After a 48-h transfection and growth for 21 days, miR-5106 expression associated with all nano-complexes was detected. At 48 h, the Au@PEI@Lipo-miR-5106 group showed significantly higher miR-5106 expression as compared with that observed in the Au@PEI-miR-5106 and Au@Lipo-miR-5106 groups, as well as for the PEI (25 kD) and Lipo groups. Additionally, miR-5106 expression for all samples was significantly increased based on culture times of up to 21 days. We also detected gradually increased miR-5106 expression in BMSC controls (negative controls without miRNA transfection) (Fig. 3(b)). The increase in miRNA expression in cells over longer culture times was also reported previously [35, 36].

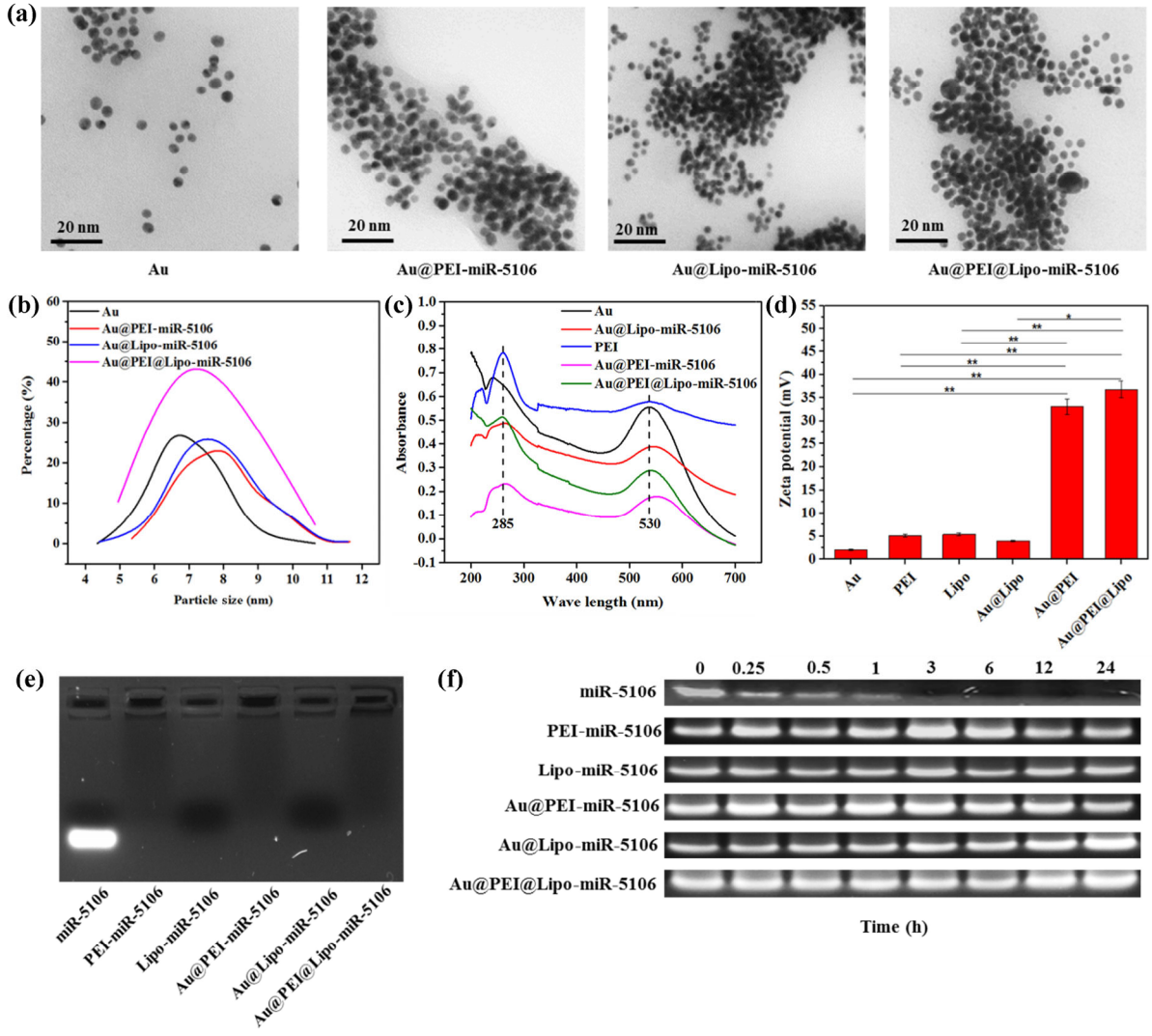

Figure 2 Characterization of USAu-miRNA nanocomplexes. (a) TEM images of various miRNA nanocomplexes (scale bar: 20 nm). (b) Size measurement of nanoparticle-miRNA complexes according to TEM images. (c) UV–vis spectra of various nanoparticles. (d) Zeta-potential analysis. *$p < 0.05$; **$p < 0.01$. (e) Agarose gel electrophoresis retardation assay for various miRNA nanocomplexes. (f) Serum stability of various miRNA nanocomplexes following incubation in 25% FBS at 37 ℃ for 0, 0.25, 0.5, 1, 3, 6, 12, and 24 h.

We also determined the cell-uptake and transfection efficiency of various nanoparticles by flow cytometry analysis (Figs. 3(c) and 3(d)). After a 24-h transfection of FAM-labeled miR-5106, we detected fluorescence intensities of 37.27%, 28.16%, 27.42%, 67.87%, and 35.54% in the PEI-miR-5106, Lipo-miR-5106, Au@PEI-miR-5106, Au@Lipo-miR-5106, and Au@PEI@Lipo-miR-5106 groups, respectively, whereas the fluorescence intensity of the negative control group with no transfected FAM-labeled miRNA was only 2.35% (Fig. 3(d)). Surface-engineered Au@Lipo-miR-5106 and Au@PEI@Lipo-miR-5106 demonstrated significantly higher degrees of cell uptake as compared with that observed with the Lipo-miR-5106 group. Therefore, our results suggested that USAuNPs can significantly improve the stability, sustained expression, and transfection efficiency of miR-5106 in cells. These findings also demonstrated the synergistic effects of Au, PEI, and Lipo on miR-5106 transfection.

3.3 Cellular biocompatibility evaluation

The cellular biocompatibility (cell viability and proliferation) of various miRNA nanocomplexes was evaluated to investigate the effect of miR-5106-loading

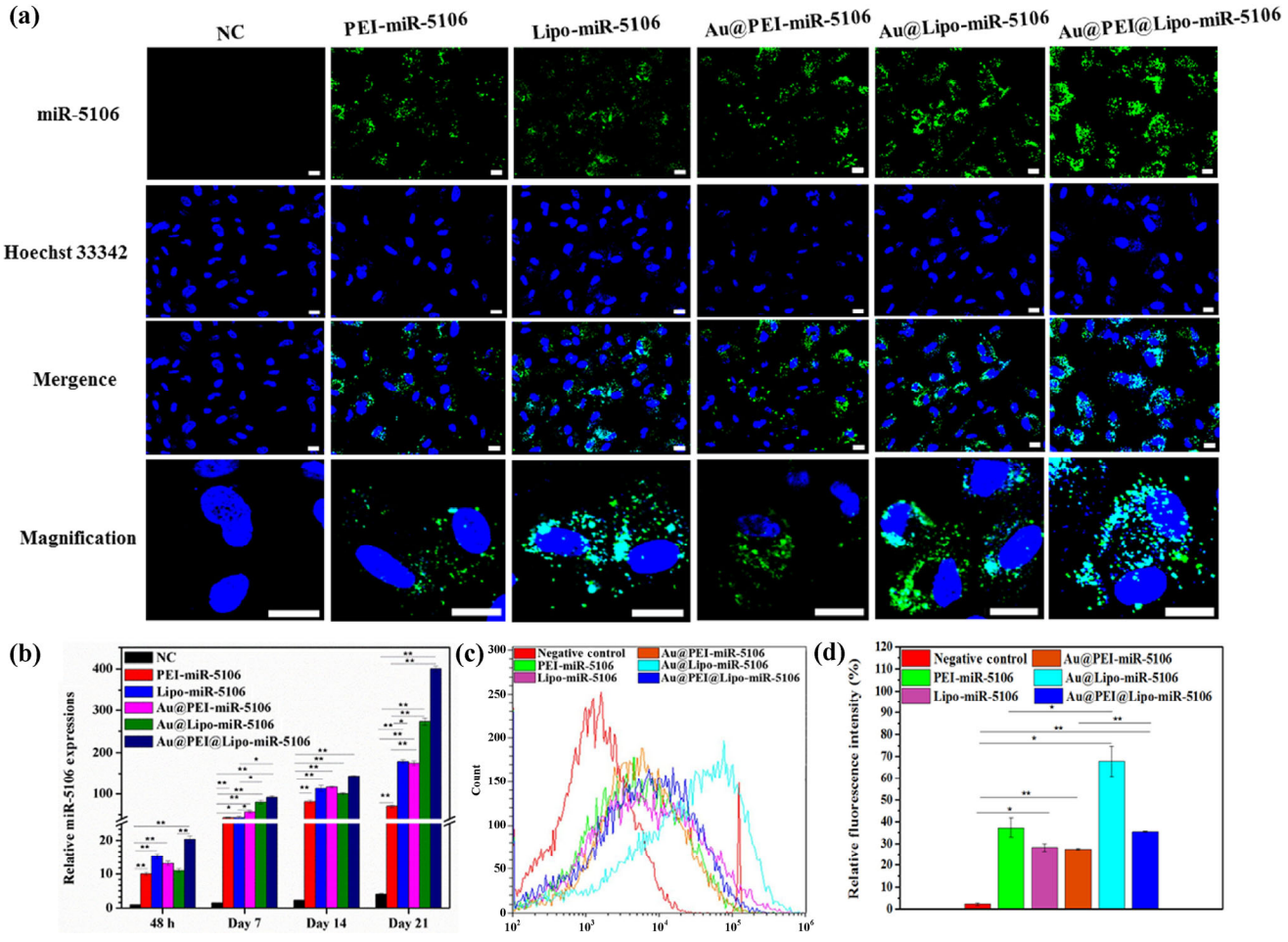

Figure 3 Intracellular transfection and delivery efficiencies of miR-5106 using various nanocomplexes. miR-5106 was FAM labeled (green), and cell nuclei were labeled by Hoechst 33342 (blue). The transfection efficiency of miR-5106 was analyzed by quantifying miR-5106 expression and cell-uptake ability. (a) Fluorescent confocal microscopy images of BMSCs following incubation with various samples loaded with miR-5106 for 24 h (scale bar: 20 μm). (b) miR-5106 expression following transfection for 24 h with various samples and detection at 48 h and 7, 14, and 21 days. (c) Flow cytometry profiles of BMSCs after a 24-h transfection with FAM-labeled miR-5106 delivered by various nanoparticles. (d) Relative fluorescence intensity of BMSCs after a 24-h incubation with various nanocomplexes based on flow cytometry results. $*p < 0.05$; $**p < 0.01$. All experiments were performed in triplicate ($n = 5$ per group).

on cytotoxicity (Fig. 4). In contrast with PEI-miR-5106 and Lipo-miR-5106, Au@PEI-miR-5106, Au@Lipo-miR-5106, and Au@PEI@Lipo-miR-5106 displayed significantly lower levels of cytotoxicity in BMSCs. Specifically, after incubation with various miRNA nanocomplexes from days 1 to 5, Au@PEI-miR-5106, Au@Lipo-miR-5106, and Au@PEI@Lipo-miR-5106 showed good cell biocompatibility, whereas PEI-miR-5106 and Lipo-miR-5106 displayed significant cytotoxicity (Fig. 4(a)); however, there were no significant differences at day 7 among the different groups. Additionally, after treatment with Au@PEI-miR-5106, Au@Lipo-miR-5106, or Au@PEI@Lipo-miR-5106 for 24 h, significantly higher numbers of living cells (green fluorescence) were observed as compared with the numbers observed following treatment with only PEI- or Lipo-miR-5106 (Fig. 4(b)). These results indicated the high cellular biocompatibility of surface-engineered USAu-miR-5106 nanoparticles, suggesting their advantages as highly efficient miRNA-delivery vectors.

3.4 Osteogenic differentiation of BMSCs following miR-5106 delivery

Surface-engineered USAuNPs were used to deliver miR-5106 into BMSCs and induce their osteogenic differentiation (Figs. 5–8). The Alp activities measured

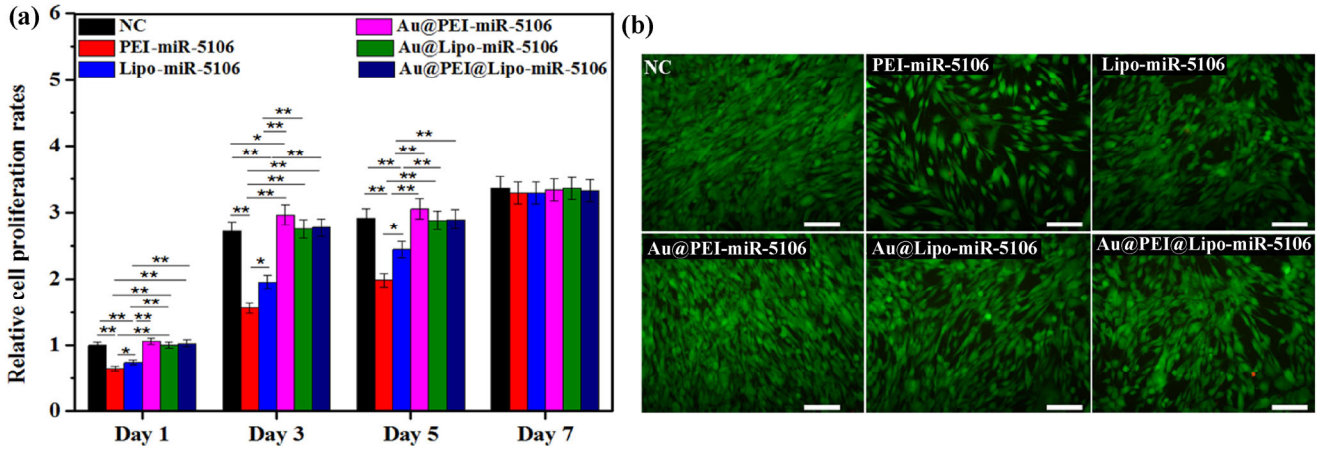

Figure 4 Cellular biocompatibility evaluation of BMSCs following incubation with various miR-5106 nanocomplexes. (a) Cell viability and proliferation after culture for 1 to 7 days. (b) Fluorescence images indicating live-dead staining after a 24-h incubation (scale bar: 100 μm). $*p < 0.05$; $**p < 0.01$. All experiments were performed in triplicate ($n = 5$ per group).

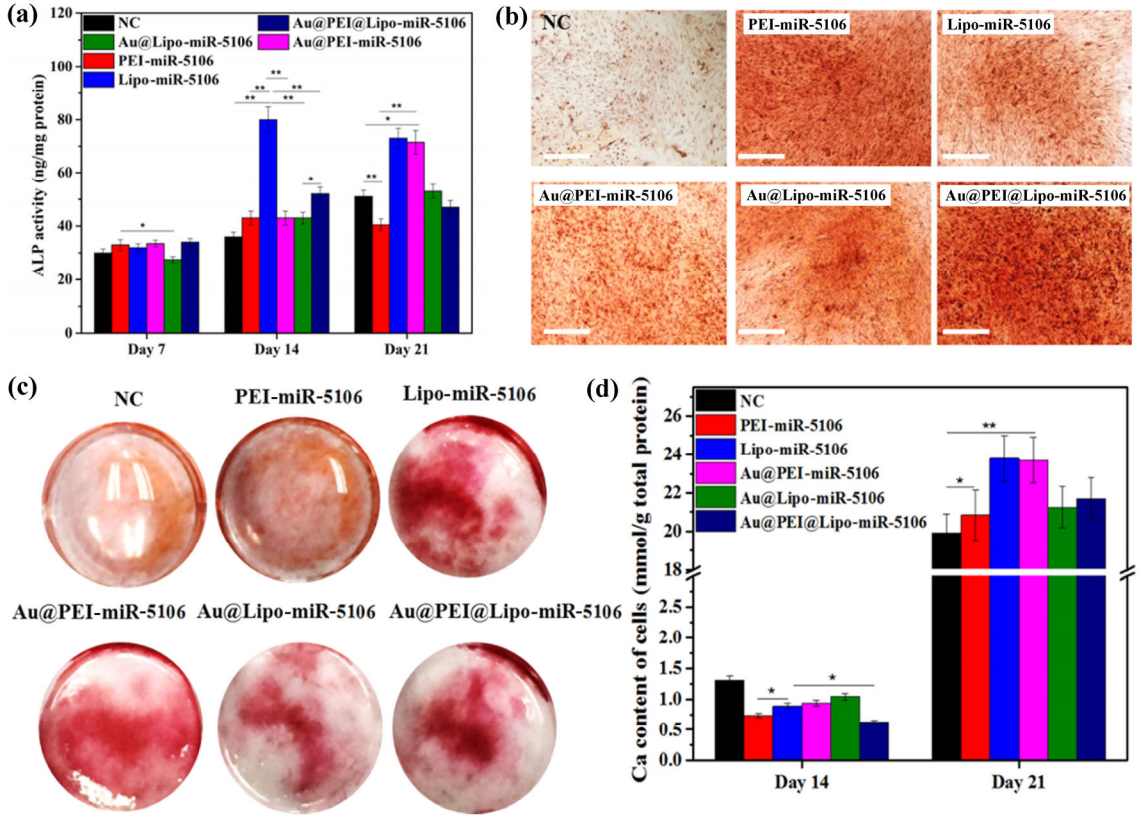

Figure 5 *In vitro* Alp activity and calcium-mineralization evaluation of BMSCs following induction by miR-5106 mimics delivered by various nanocomplexes. (a) Alp activity on days 7, 14, and 21. (b) and (c) Alizarin red staining of cells (scale bar: 200 μm) (b) and 24 well-plates (c) on day 21. (d) Calcium- content determination at different time points (14 and 21 days). $*p < 0.05$; $**p < 0.01$. All experiments were performed in triplicate ($n = 5$ per group).

in BMSCs following induction by miR-5106 nanocomplexes were detected at days 7, 14, and 21 (Fig. 5(a)). Alp activity in all samples increased at culture times of up to 14 days. On day 7, BMSCs incubated with Au@PEI@Lipo-miR-5106 showed significantly higher Alp activity as compared with that observed in BMSCs incubated with Au@Lipo-miR-5106, with no significant differences observed between other samples.

After culture for 14 days, Au@PEI@Lipo-miR-5106 significantly enhanced Alp activity in BMSCs as compared with that observed in negative controls and PEI-miR-5106, Au@PEI-miR-5106, and Au@Lipo-miR-5106 groups. The Alp activity in BMSCs did not increase on day 21, regardless of nanoparticle incubation. The observed alterations in Alp activity between these samples were consistent with previous reports [37].

The calcium deposition and mineralization of BMSCs transfected with various miR-5106 nanocomplexes were detected by alizarin red stain and calcium-content examination (Figs. 5(b)–5(d). Compared with negative controls, after a 21-day incubation with nanocomplexes, miR-5106-transfected groups showed significantly stronger alizarin red staining, suggesting high levels of calcium mineralization (Figs. 5(b) and 5(c)). Calcium-content detection in BMSCs was performed following transfection with various miRNA nanocomplexes for 14 and 21 days (Fig. 5(d)). We observed no significant difference in calcium content between the different groups on day 14; however, on day 21, the calcium content from disrupted cells was significantly enhanced by Lipo-miR-5106, Au@PEI-miR-5106, or Au@PEI@Lipo-miR-5106 transfection relative to levels observed in negative controls. The results from alizarin red staining and calcium-content analysis suggested that our optimized surface-engineered USAu-miR-5106 complexes significantly improved BMSC mineralization capability.

To demonstrate the effect of miR-5106 transfection on BMSC osteogenic differentiation at the mRNA level, we determined the expression of osteoblastic genes (early-stage markers: *Alp* and *Runx*2; late-stage mineralization marker: *Ocn*) in cells following transfection with various miR-5106 nanocomplexes (Fig. 6). *Alp* expression in all samples continued to increase from days 7 to 14, reaching peak values at day 14

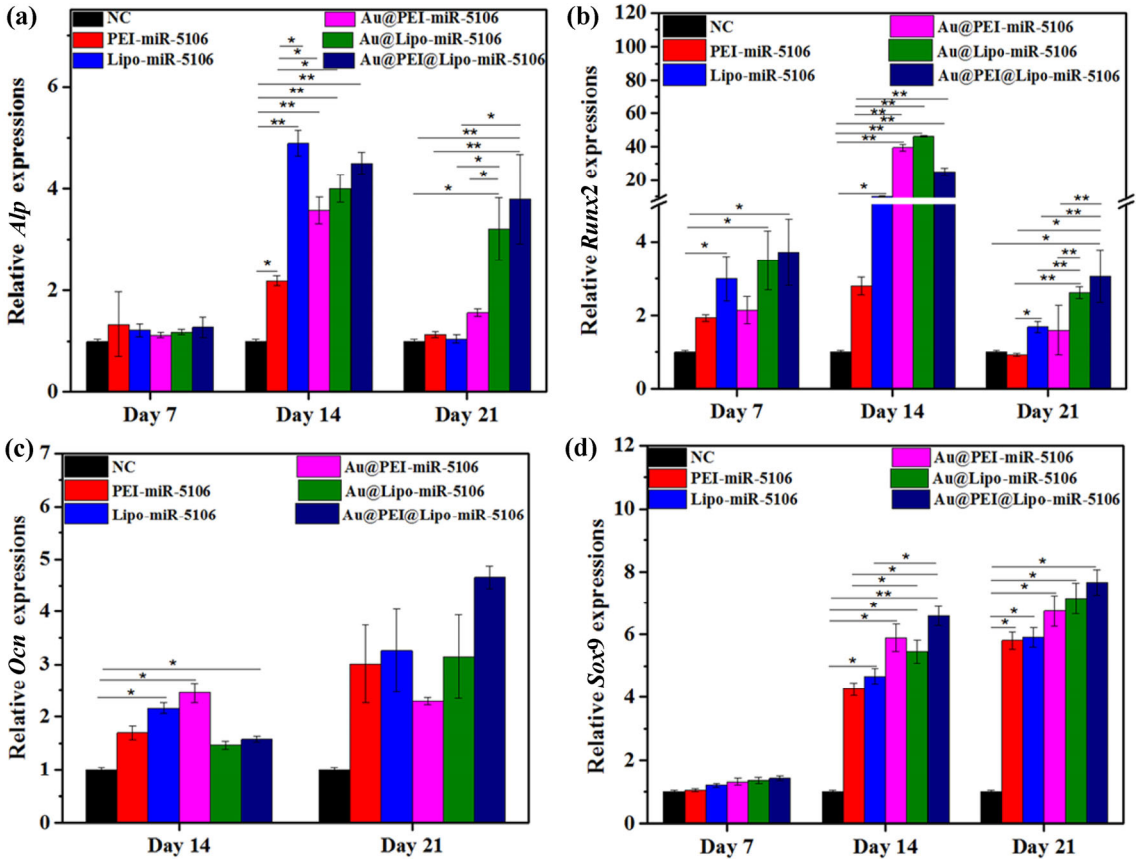

Figure 6 Osteoblastic marker-gene expressions during osteogenic differentiation following induction by various miR-5106 nanocomplexes on days 7, 14, and 21. Expression levels of (a) *Alp*, (b) *Runx*2, (c) *Ocn*, and (d) *Sox*9. All gene-expression data were normalized to *Gapdh*, and the expression levels in sample groups were relative to those of the negative control. *$p < 0.05$; **$p < 0.01$. All experiments were performed in triplicate ($n = 5$ per group).

before beginning to decrease at day 21 (Fig. 6(a)). There were no significant differences in *Alp* expression observed between various groups on day 7; however, on day 14, cells transfected with Au@PEI@Lipo-miR-5106 showed significantly higher *Alp* expression as compared with that observed in negative controls and cells transfected with PEI-miR-5106, Au@PEI-miR-5106, or Au@Lipo-miR-5106. On day 21, cells transfected with Au@PEI@Lipo-miR-5106 continued to exhibit high *Alp*-expression levels as compared with other groups (Fig. 6(a)). *Runx*2 expression was significantly upregulated following transfection with Au-based miR-5106 nanocomplexes over all culture time periods (Fig. 6(b)). On day 21, Au@PEI@Lipo-miR-5106 showed significantly higher *Ocn* expression as compared with the other groups, including cells transfected with Lipo-miR-5106 (Fig. 6(c)); however, on day 7, *Ocn* expression was not detected in any group. As a miR-5106-target gene, *Sox*9 expression was also upregulated during the osteogenic differentiation period, especially in Au@PEI-miR-5106-, Au@Lipo-miR-5106-, and Au@PEI@Lipo-miR-5106-transfected cells (Fig. 6(d)). On days 14 and 21, significantly higher *Sox*9 expression was observed in Au@PEI@Lipo-miR-5106-transfected cells as compared with negative controls, Lipo-miR-5106-, PEI-miR-5106-, and Au@PEI-miR-5106-transfected cells.

Additionally, immunofluorescence staining for *Runx*2 and *Ocn* proteins on day 21 (Figs. 7 and 8) revealed that all groups were positive for *Runx*2 and *Ocn*, although there were differences in fluorescence intensity (Figs. 7(a) and 8(a)). Specifically, the Au@PEI@Lipo-miR-5106 group showed significantly higher fluorescence intensity associated with *Runx*2 expression as compared with that observed in PEI-miR-5106-transfected cells and comparable intensity relative to that observed in Lipo-miR-5106-tranfected cells (Fig. 7(b)). The Au@PEI@Lipo-miR-5106 group exhibited significantly higher fluorescence intensity associated with *Ocn* expression as compared to that observed in negative controls, PEI-miR-5106-, Lipo-miR-5106-, and Au@PEI-miR-5106-transfected cells (Fig. 8(b)). Therefore, these results indicated that the optimized surface-engineered AuNP-miR-5106 nanocomplexes significantly enhanced osteogenic protein expression. Furthermore, Alp activity, calcium deposition, and

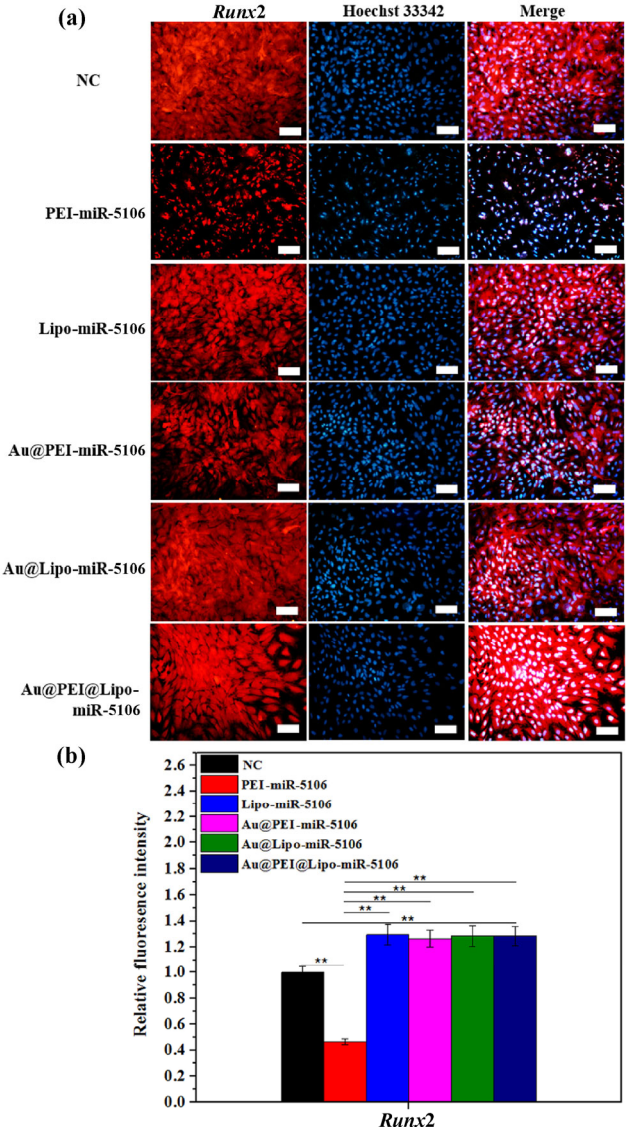

Figure 7 Immunofluorescence staining for the *Runx*2 protein in BMSCs on day 21 following transfection of miR-5106 through various nanoparticles. (a) Immunofluorescence visualizing the *Runx*2 protein. (b) Quantified fluorescence intensity of *Runx*2 expression (scale bar: 100 μm). $*p < 0.05$; $**p < 0.01$.

gene-expression results demonstrated that miR-5106 significantly enhanced osteogenic differentiation of BMSCs through optimized AuNP-based delivery.

3.5 Mechanisms associated with BMSC differentiation mediated by USAu-based miR-5106 delivery

To overcome miRNA-related clinical limitations, such as short half-life and biological stability, we developed a highly efficient miRNA-delivery system exhibiting low levels of cytotoxicity based on USAu@PEI@Lipo

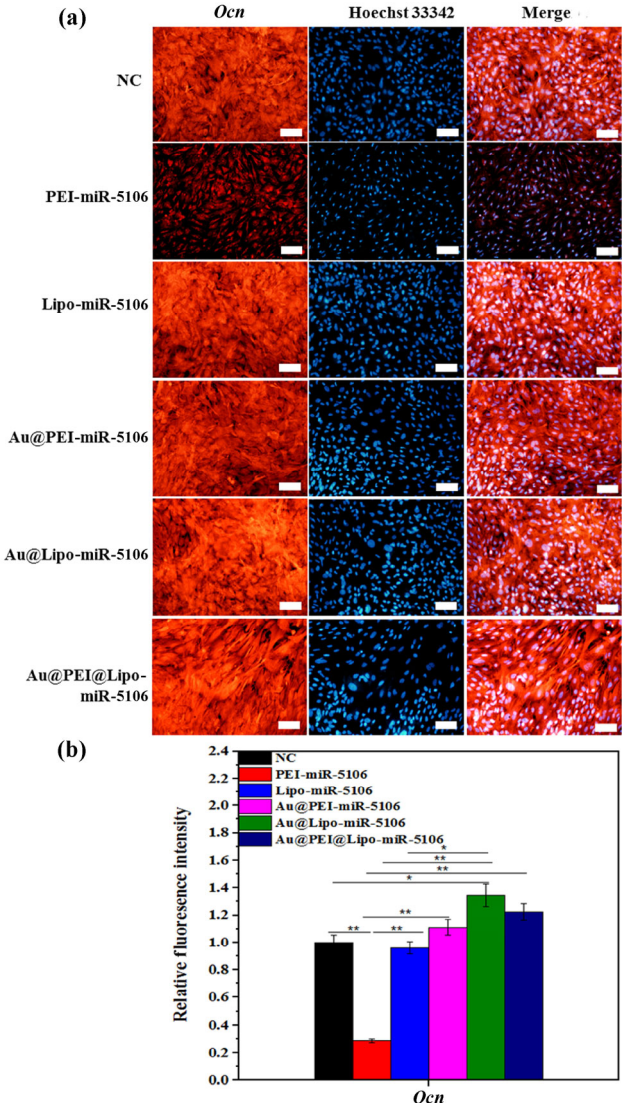

Figure 8 Immunofluorescence staining for the *Ocn* protein in BMSCs on day 21 following transfection of miR-5106 through various nanoparticles. (a) Immunofluorescence visualizing the *Ocn* protein. (b) Quantified fluorescence intensity of *Ocn* expression. Significantly higher *Ocn* expression was observed in BMSCs transfected with miR-5106 via optimized surface-engineered USAuNPs (scale bar: 100 μm). *$p < 0.05$; **$p < 0.01$.

nanoparticles. To improve miRNA delivery, the surface of AuNPs was coated with commercial PEI (25 kD) and Lipo by layer-by-layer assembly technology. Compared with commercial PEI and Lipo, the optimized Au@PEI@Lipo nanoparticles showed enhanced miRNA-loading and -delivery capabilities, as well as negligible cytotoxicity. Additionally, nanoparticle-mediated miR-5106 delivery significantly enhanced the osteoblastic differentiation of BMSCs *in vitro*. These results demonstrated that our optimized Au@PEI@Lipo nanoparticles could serve as highly efficient gene vectors for bone tissue-regeneration applications.

Owing to the non-biodegradable nature of inorganic nanocrystals and their rapid uptake by the reticuloendothelial system, nanocrystals with sizes > 10 nm instill concerns regarding increased long-term toxicity [38]. As compared to organic nanoparticles, inorganic nanoplatforms capable of controlled biodegradation or renal clearance may be promising for future clinical transformation. Fortunately, recent ultra-small inorganic crystals (<10 nm), including quantum dots and AuNPs, exhibited properties enabling rapid renal clearance [39, 40]. Compared with quantum dots, AuNPs possess good biocompatibility and stability for biomedical applications. Therefore, AuNPs constitute promising non-viral vectors for gene delivery, especially through their ability to improve gene stability and delivery efficiency [41]. PEI-conjugated AuNPs exhibited significantly higher DNA- and siRNA-delivery efficiency as compared with commercial PEI (25 kD) [42, 43]. Most surface-engineered Au@PEI nanoparticles > 10 nm are used as DNA or siRNA vectors for cancer therapy; however, few studies have reported AuNP-mediated miRNA delivery to control BMSC osteogenic differentiation. In our study, USAuNPs were surface engineered by PEI and Lipo using layer-by-layer assembly to form optimized Au@PEI@Lipo nanoparticles, which were used to deliver miR-5106 into BMSCs and regulate their osteogenic differentiation. As compared with commercial Lipo and PEI (25 kD), our surface-engineered USAuNPs showed significantly higher miRNA-delivery efficiency and osteogenic differentiation activity, as well as low levels of cytotoxicity.

Generally, miRNAs target mRNAs and suppress their translation by promoting their degradation [44]. However, in our study, we found that the osteogenic activity associated with miR-5106 occurred through targeting and increasing Sox9 activity rather than through suppression of a specific target gene. To demonstrate the role of miR-5106 in regulating BMSC differentiation, we performed target-gene prediction and investigated the interaction mechanism of miR-5106

by luciferase-reporter assay as shown in Fig. S1 (in the ESM). Computational algorithms predicted that *Sox*9 was the candidate target likely to interact with the 3′UTR of miR-5106 (Fig. S1(a) in the ESM). To explore whether *Sox*9 was a miR-5106 target, the *Sox*9 3′UTR was inserted downstream from the Renilla luciferase-coding region in the reporter vector (Fig. S1(b) in the ESM). Compared with negative controls and miR-5106-knockdown cells, we observed a 27% suppression of luciferase activity following co-transfection with miR-5106 mimics and the *Sox*9-3′UTR reporter vector, indicating that *Sox*9 was a target of miR-5106 (Fig. S1(c) in the ESM).

In regenerative medicine and cancer therapy, therapeutic gene modalities, including DNA, siRNA, and miRNA, play important roles and have shown promising application potential. However, significant obstacles in the application of gene therapy involve their safe and highly efficient delivery, cellular uptake, and biological stability [45, 46]. Here, the surface-engineered USAuNPs developed in this study demonstrated significantly low levels of cytotoxicity along with highly efficient delivery of miRNA to cells in order to regulate stem cell fate. As a novel non-viral vector, this nanoplatform could also deliver other genes for biomedical applications, such as tissue regeneration and disease treatment. The *in vivo* osteogenic mechanism and capabilities associated with this USAu-based miRNA-delivery platform will be expanded upon in future studies.

4 Conclusion

In conclusion, USAuNPs were successfully surface engineered using PEI and Lipo layer-by-layer assembly. The optimized Au@PEI@Lipo nanoplatforms showed high miR-5106-transfection efficiency, stable expression in cells, excellent cellular uptake, and low levels of cytotoxicity as compared with commercial PEI (25 kD) and Lipo. Additionally, cells transfected with miR-5106 via optimized Au@PEI@Lipo systems significantly enhanced the osteogenic differentiation ability of BMSCs through gene targeting, thereby enhancing Sox9 activity. The surface-engineering strategy described here could also be applied to design other ultra-small inorganic nanoparticles as highly efficient therapeutic nucleic acid-delivery systems for tissue regeneration and disease therapy.

Acknowledgements

We acknowledge the valuable comments of potential reviewers. This work was supported by State Key Laboratory for Mechanical Behavior of Materials, the Scientific Research Starting Foundation from Xi'an Jiaotong University (No. DW011798N3000010), the Fundamental Research Funds for the Central Universities (No. XJJ2014090), the Natural Science Basic Research Plan in Shaanxi Province of China (No. 2015JQ5165), and National Natural Science Foundation of China (No. 51502237).

Electronic Supplementary Material: Supplementary material (primers used in RT-PCR analysis and target genes evaluations) is available in the online version of this article at http://dx.doi.org/10.1007/s12274-016-1265-9.

References

[1] Oliveira, J. M.; Rodrigues, M. T.; Silva, S. S.; Malafaya, P. B.; Gomes, M. E.; Viegas, C. A.; Dias, I. R.; Azevedo, J. T.; Mano, J. F.; Reis, R. L. Novel hydroxyapatite/chitosan bilayered scaffold for osteochondral tissue-engineering applications: Scaffold design and its performance when seeded with goat bone marrow stromal cells. *Biomaterials* **2006**, *27*, 6123–6137.

[2] Zhu, Y.; Mao, Z. W.; Gao, C. Y. Control over the gradient differentiation of rat BMSCs on a PCL membrane with surface-immobilized alendronate gradient. *Biomacromolecules* **2013**, *14*, 342–349.

[3] Lewis, B. P.; Burge, C. B.; Bartel, D. P. Conserved seed pairing, often flanked by adenosines, indicates that thousands of human genes are microRNA targets. *Cell* **2005**, *120*, 15–20.

[4] Stegen, S.; van Gastel, N.; Carmeliet, G. Bringing new life to damaged bone: The importance of angiogenesis in bone repair and regeneration. *Bone* **2015**, *70*, 19–27.

[5] Li, Y.; Fan, L. K.; Liu, S. Y.; Liu, W. J.; Zhang, H.; Zhou, T.; Wu, D.; Yang, P.; Shen, L. J.; Chen, J. H. et al. The promotion of bone regeneration through positive regulation of angiogenic–osteogenic coupling using microRNA-26a. *Biomaterials* **2013**, *34*, 5048–5058.

[6] Zhang, X. J.; Li, Y.; Chen, Y. E.; Chen, J. H.; Ma, P. X. Cell-free 3D scaffold with two-stage delivery of miRNA-26a to regenerate critical-sized bone defects. *Nat. Commun.* **2016**, *7*, 10376.

[7] Kai, Z. S.; Pasquinelli, A. E. MicroRNA assassins: Factors that regulate the disappearance of miRNAs. *Nat. Struct. Mol. Biol.* **2010**, *17*, 5–10.

[8] Bozzuto, G.; Molinari, A. Liposomes as nanomedical devices. *Int. J. Nanomedicine* **2015**, *10*, 975–999.

[9] Pattni, B. S.; Chupin, V. V.; Torchilin, V. P. New developments in liposomal drug delivery. *Chem. Rev.* **2015**, *115*, 10938–10966.

[10] Yin, H.; Kanasty, R. L.; Eltoukhy, A. A.; Vegas, A. J.; Dorkin, J. R.; Anderson, D. G. Non-viral vectors for gene-based therapy. *Nat. Rev. Genet.* **2014**, *15*, 541–555.

[11] Wang, W.; Li, W.; Ma, N.; Steinhoff, G. Non-viral gene delivery methods. *Curr. Pharm. Biotechnol.* **2013**, *14*, 46–60.

[12] Arote, R.; Kim, T.-H.; Kim, Y.-K.; Hwang, S.-K.; Jiang, H.-L.; Song, H.-H.; Nah, J.-W.; Cho, M.-H.; Cho, C.-S. A biodegradable poly(ester amine) based on polycaprolactone and polyethylenimine as a gene carrier. *Biomaterials* **2007**, *28*, 735–744.

[13] Xiong, M. P.; Forrest, M. L.; Ton, G.; Zhao, A. N.; Davies, N. M.; Kwon, G. S. Poly(aspartate-g-PEI800), a polyethylenimine analogue of low toxicity and high transfection efficiency for gene delivery. *Biomaterials* **2007**, *28*, 4889–4900.

[14] Conde, J.; Edelman, E. R.; Artzi, N. Target-responsive DNA/RNA nanomaterials for microRNA sensing and inhibition: The jack-of-all-trades in cancer nanotheranostics? *Adv. Drug Deliv. Rev.* **2015**, *81*, 169–183.

[15] Dong, H. F.; Dai, W. H.; Ju, H. X.; Lu, H. T.; Wang, S. Y.; Xu, L. P.; Zhou, S.-F.; Zhang, Y.; Zhang, X. J. Multifunctional poly(L-lactide)–polyethylene glycol-grafted graphene quantum dots for intracellular microrna imaging and combined specific-gene-targeting agents delivery for improved therapeutics. *ACS Appl. Mater. Interfaces* **2015**, *7*, 11015–11023.

[16] Wang, X. L.; Lai, Y. X.; Ng, H. H.; Yang, Z. J.; Qin, L. Systemic drug delivery systems for bone tissue regeneration—A mini review. *Curr. Pharm. Des.* **2015**, *21*, 1575–1583.

[17] Wang, Y. D.; Zern, B.; Gumera, C. Biomimetic Polymers and Uses Thereof. U.S. Patent 8,529,928, Sep 10, 2013.

[18] Ding, Y.; Jiang, Z. W.; Saha, K.; Kim, C. S.; Kim, S. T.; Landis, R. F.; Rotello, V. M. Gold nanoparticles for nucleic acid delivery. *Mol. Ther.* **2014**, *22*, 1075–1083.

[19] Almeida, J. P. M.; Figueroa, E. R.; Drezek, R. A. Gold nanoparticle mediated cancer immunotherapy. *Nanomedicine* **2014**, *10*, 503–514.

[20] Austin, L. A.; Mackey, M. A.; Dreaden, E. C.; El-Sayed, M. A. The optical, photothermal, and facile surface chemical properties of gold and silver nanoparticles in biodiagnostics, therapy, and drug delivery. *Arch. Toxicol.* **2014**, *88*, 1391–1417.

[21] Ghosh, R.; Singh, L. C.; Shohet, J. M.; Gunaratne, P. H. A gold nanoparticle platform for the delivery of functional microRNAs into cancer cells. *Biomaterials* **2013**, *34*, 807–816.

[22] Wang, H. Y.; Jiang, Y. F.; Peng, H. G.; Chen, Y. Z.; Zhu, P. Z.; Huang, Y. Z. Recent progress in microRNA delivery for cancer therapy by non-viral synthetic vectors. *Adv. Drug Deliv. Rev.* **2015**, *81*, 142–160.

[23] Bishop, C. J.; Tzeng, S. Y.; Green, J. J. Degradable polymer-coated gold nanoparticles for co-delivery of DNA and siRNA. *Acta Biomater.* **2015**, *11*, 393–403.

[24] Longmire, M.; Choyke, P. L.; Kobayashi, H. Clearance properties of nano-sized particles and molecules as imaging agents: Considerations and caveats. *Nanomedicine* **2008**, *3*, 703–717.

[25] Wang, B.; He, X.; Zhang, Z. Y.; Zhao, Y. L.; Feng, W. Y. Metabolism of nanomaterials *in vivo*: Blood circulation and organ clearance. *Acc. Chem. Res.* **2013**, *46*, 761–769.

[26] Karmali, P. P.; Simberg, D. Interactions of nanoparticles with plasma proteins: Implication on clearance and toxicity of drug delivery systems. *Expert Opin. Drug Deliv.* **2011**, *8*, 343–357.

[27] Zhang, X.-D.; Wu, D.; Shen, X.; Liu, P.-X.; Yang, N.; Zhao, B.; Zhang, H.; Sun, Y.-M.; Zhang, L.-A.; Fan, F.-Y. Size-dependent *in vivo* toxicity of PEG-coated gold nanoparticles. *Int. J. Nanomedicine* **2011**, *6*, 2071–2081.

[28] Zhang, X.-D.; Wu, D.; Shen, X.; Liu, P.-X.; Fan, F.-Y.; Fan, S.-J. *In vivo* renal clearance, biodistribution, toxicity of gold nanoclusters. *Biomaterials* **2012**, *33*, 4628–4638.

[29] Dreaden, E. C.; Morton, S. W.; Shopsowitz, K. E.; Choi, J.-H.; Deng, Z. J.; Cho, N.-J.; Hammond, P. T. Bimodal tumor-targeting from microenvironment responsive hyaluronan layer-by-layer (LbL) nanoparticles. *ACS Nano* **2014**, *8*, 8374–8382.

[30] Sun, Q.; Kang, Z. S.; Xue, L. J.; Shang, Y. K.; Su, Z. G.; Sun, H. B.; Ping, Q. N.; Mo, R.; Zhang, C. A collaborative assembly strategy for tumor-targeted siRNA delivery. *J. Am. Chem. Soc.* **2015**, *137*, 6000–6010.

[31] Gao, C. B.; Vuong, J.; Zhang, Q.; Liu, Y. D.; Yin, Y. D. One-step seeded growth of Au nanoparticles with widely tunable sizes. *Nanoscale* **2012**, *4*, 2875–2878.

[32] Link, S.; El-Sayed, M.-A. Size and temperature dependence of the plasmon absorption of colloidal gold nanoparticles. *J. Phys. Chem. B* **1999**, *103*, 4212–4217.

[33] Lee, Y.; Lee, S.-H.; Kim, J.-S.; Maruyama, A.; Chen, X. S.; Park, T.-G. Controlled synthesis of PEI-coated gold nanoparticles using reductive catechol chemistry for siRNA

delivery. *J. Control. Release* **2011**, *155*, 3–10.

[34] Elbakry, A.; Zaky, A.; Liebl, R.; Rachel, R.; Goepferich, A.; Breunig, M. Layer-by-layer assembled gold nanoparticles for siRNA delivery. *Nano Lett.* **2009**, *9*, 2059–2064.

[35] Fontana, L.; Pelosi, E.; Greco, P.; Racanicchi, S.; Testa, U.; Liuzzi, F.; Croce, C. M.; Brunetti, E.; Grignani, F.; Peschle, C. MicroRNAs *17–5p-20a-106a* control monocytopoiesis through AML1 targeting and M-CSF receptor upregulation. *Nat. Cell Biol.* **2007**, *9*, 775–787.

[36] Huang, X.; Gschweng, E.; Van Handel, B.; Cheng, D.; Mikkola, H. K.; Witte, O. N. Regulated expression of microRNAs-126/126* inhibits erythropoiesis from human embryonic stem cells. *Blood* **2011**, *117*, 2157–2165.

[37] Boanini, E.; Torricelli, P.; Gazzano, M.; Della Bella, E.; Fini, M.; Bigi, A. Combined effect of strontium and zoledronate on hydroxyapatite structure and bone cell responses. *Biomaterials* **2014**, *35*, 5619–5626.

[38] Ehlerding, E. B.; Chen, F.; Cai, W. B. Biodegradable and renal clearable inorganic nanoparticles. *Adv. Sci.* **2016**, 3, 1500223.

[39] Choi, H. S.; Liu, W. B.; Misra, P.; Tanaka, E.; Zimmer, J. P.; Itty Ipe, B.; Bawendi, M. G.; Frangioni, J. V. Renal clearance of quantum dots. *Nat. Biotechnol.* **2007**, *25*, 1165–1170.

[40] Yu, M. X.; Zheng, J. Clearance pathways and tumor targeting of imaging nanoparticles. *ACS Nano* **2015**, *9*, 6655–6674.

[41] Rana, S.; Bajaj, A.; Mout, R.; Rotello, V. M. Monolayer coated gold nanoparticles for delivery applications. *Adv. Drug Deliv. Rev.* **2012**, *64*, 200–216.

[42] Tian, H. Y.; Guo, Z. P.; Chen, J.; Lin, L.; Xia, J. J.; Dong, X.; Chen, X. S. PEI conjugated gold nanoparticles: Efficient gene carriers with visible fluorescence. *Adv. Healthc. Mater.* **2012**, *1*, 337–341.

[43] Shen, J. L.; Kim, H. C.; Mu, C. F.; Gentile, E.; Mai, J. H.; Wolfram, J.; Ji, L. N.; Ferrari, M.; Mao, Z. W.; Shen, H. F. Multifunctional gold nanorods for siRNA gene silencing and photothermal therapy. *Adv. Healthc. Mater.* **2014**, *3*, 1629–1637.

[44] Valencia-Sanchez, M. A.; Liu, J. D.; Hannon, G. J.; Parker, R. Control of translation and mRNA degradation by miRNAs and siRNAs. *Genes Dev.* **2006**, *20*, 515–524.

[45] Peng, B.; Chen, Y. M.; Leong, K. W. MicroRNA delivery for regenerative medicine. *Adv. Drug Deliv. Rev.* **2015**, *88*, 108–122.

[46] Yang, J. P.; Zhang, Q.; Chang, H.; Cheng, Y. Y. Surface-engineered dendrimers in gene delivery. *Chem. Rev.* **2015**, *115*, 5274–5300.